Metallic salt deposition on porous particles by dry impregnation in fluidized bed: Effect of drying conditions on metallic nanoparticles distribution

L. Barthe, S. Desportes, D. Steinmetz, M. Hemati*

Laboratoire de Génie Chimique, UMR CNRS 5503-INP-ENSIACET, 5 rue Paulin Talabot, BP 1301, 31106 Toulouse Cedex 01, France

A B S T R A C T

In this paper, the fluidized bed dry impregnation of coarse alumina porous particles by a metallic salt, manganese nitrate, is investigated. In this technique the penetration of each drop of metallic solution in the porous solid particle and solvent evaporation takes place at the same time, then liquid diffusion phenomenon is negligible. So, the metal loading is directly related to the operating time and liquid flow rate and concentration.

It is found that the competition between two phenomena, drying and capillary flow, controls the deposit location. In order to determine the importance of the solvent evaporation process compared to the solution penetration by capillarity, an impregnation module, IM, was defined as the ratio between the drying characteristic time and a capillary penetration time. The adequate choice of the operating conditions (bed temperature, liquid and fluidization gas flow rate) allows a uniform deposition of the metallic precursor inside the porous matrix or on the support surface. The impregnation under slow drying conditions ($IM \geq 10$ and solvent content in the bed atmosphere $\tau_s \geq 0.2$) leads to a homogeneous deposition inside the pores. Under fast drying conditions ($IM < 5$ and $\tau_s < 0.2$), the deposit is located at the particle external surface.

In the case of slow drying, the impregnation kinetics can be represented by a "shrinking core" model. The critical impregnation rate is controlled by the competition between dissolution and recrystallization at the elementary grain scale. The size of the metal crystallites depends on the pore mean size and size distribution and on the drying rate.

Keywords: Drying; Dry impregnation; Fluidized bed; Capillary flow; Shrinking core model; Metallic nanoparticles

1. Introduction

The usual preparation methods of supported catalysts consist in several steps such as impregnation, filtration, drying and calcination/activation. The literature studies show that, if there is no strong interaction between the support and the impregnation solution, the drying step determines the deposit location and dispersion in the porous matrix (Fulton, 1986; Lekhal et al., 2001).

The dry impregnation and activation in fluidized bed can be considered as a new and alternative technique. It was elaborated in Laboratoire de Génie Chimique de Toulouse and patented by INP/CNRS (Patent EPI-PCT/FR 02/01795). This method is a "one pot process", which allows achieving in the same apparatus:

- The dry impregnation of hot fluidized porous particles by a spraying metallic precursor solution.
- The precursor decomposition and the metal activation by heating the impregnated support in a reducing atmosphere.

During the dry impregnation step, the pulverized solution penetrates inside the porous support by capillarity (liquid spreading/penetration), and in the same time the solvent is evaporated thanks to the energy brought by the fluidization gas (drying). These phenomena depend on:

* *Corresponding author*.
E-mail addresses: Laurie.Barthe@ensiacet.fr (L. Barthe), Mehrdji.Hemati@ensiacet.f (M. Hemati).

- The process related variables (fluidization gas flow rate, bed temperature, atomizing gas and liquid flow rates, and atomizer location).
- The physicochemical properties (liquid interfacial tension, liquid viscosity, contact angle between solid and liquid, nature and texture of solid particles).

The interdependency between these two sets of parameters determines the product quality and the metal repartition into the porous particles.

Few studies are reported on the dry impregnation technique. A previous work (Desportes, 2005; Barthe et al., 2007) was realized in our laboratory, on dry impregnation of porous particles (alumina and silica) with aqueous solutions of sodium chloride, manganese nitrate and sodium carboxymethylcellulose. It showed that, at low bed temperatures ($T \leq 50\,^{\circ}C$), the precursor is deposited essentially inside the pore volume (non-growth period). The growth phenomenon does not arise before the full filling of internal porosity.

These results can be explained by large value of the capillary tension given by Laplace's equation:

$$p_c = \frac{2\gamma_{LV}\cos\theta}{r_{pore}} \quad (1)$$

where r_{pore} represents the pore radius, γ_{LV}, the interfacial tension, and θ the contact angle.

When the liquid wets perfectly the solid surface ($\theta = 0$), this equation leads to high values of the capillary tension for mean pore radius less than 100 Å.

The time necessary for liquid penetration in the pores, t_{cap}, can be estimated from the following equation taken from the model of the parallel capillary beam (Burdine, 1953):

$$t_{cap} = \frac{2\mu x^2}{\gamma_{LV}\cos\theta r_{pore}} \quad (2)$$

where μ is the liquid viscosity and x the pore length equivalent to the radius particle multiplied by the tortuosity factor.

Thanks to these capillary phenomena, if the external exchange potential is low, the liquid sprayed on the porous particles surface can migrate inside the support before drying leads to pores blocking. The external exchange potential depends both on solvent partial pressure at the solid/gas interface and on the solvent partial pressure in the fluidized bed. Under these conditions, a fast evaporation of solvent is avoided when liquid drops and solid particles are in contact.

In the fluidized bed, impregnation and drying take place simultaneously (dry impregnation). So, similarly to the capillary characteristic time, a time relative to the drying phenomenon was considered. The drying time, t_{dry}, is defined as the time necessary for a particle saturated by pure solvent to be transformed into a dry particle under defined fluidized bed conditions (temperature and humidity). The calculation of this characteristic time is based on the mass and energy balances on a single wetted particle considering that the mass transfer is controlled by external resistance (gas phase). The model's equations described in previous works (Barthe et al., 2007; Desportes, 2005) lead to this last equation:

$$t_{dry} = \frac{d_p \chi \rho_s}{6k_y(Y_i - \bar{Y})} \quad (3)$$

where d_p is the particle diameter, χ the internal support porosity, ρ_s the solvent density, k_y the overall mass transfer coefficient, $\bar{Y}$ the average solvent content in the bed atmosphere determined by overall mass balance on the reactor, and Y_i the absolute solvent content at the interface (depending on the particle temperature and humidity (Barthe et al., 2007)).

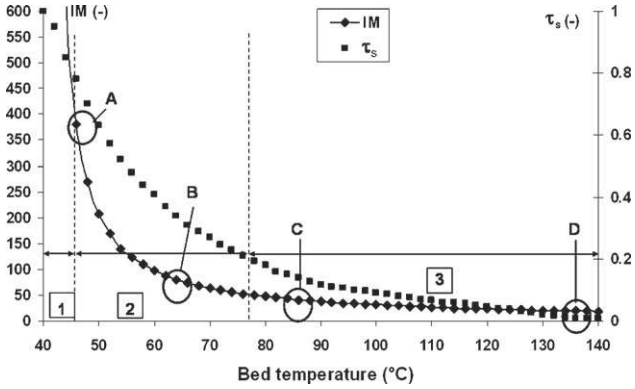

Fig. 1 – IM and saturation rate evolution versus bed temperature (impregnation of fine silica particles by iron).

In order to estimate the preponderance of the drying phenomenon compared to capillarity, an impregnation module was defined, IM, as the ration between these two characteristic times:

$$IM = \frac{t_{dry}}{t_{cap}} \quad (4)$$

The precursor distribution can be considered as uniform when IM becomes higher than a critical value proposed by (Desportes et al., 2005; Barthe et al., 2007) and presented hereafter.

Different feasibility tests were carried out in these studies using various fine porous particles (Al_2O_3 and SiO_2 particles with mean diameter $d_p \approx 100\,\mu m$) and metallic precursor solutions prepared from inorganic salts or organometallic complexes.

For example, in the case of the impregnation of fine porous silica particles ($d_p \approx 120\,\mu m$) by an iron nitrate solution, four sets of experiments were carried out corresponding to slow, intermediate and fast drying conditions (Barthe, 2007). Fig. 1 shows, for a fixed impregnation liquid flow rate, the prediction by the previous model concerning the effect of bed temperature on IM and solvent vapour saturation rate, τ_s.

On this figure three different zones can be distinguished:

- The first zone, known as "unstable zone", is observed for high τ_s (between 1 and 0.8) and it is characterized by a fast decrease of IM. In this zone, the operation is unstable: a weak increase of the liquid flow rate, or a light reduction of the inlet gas temperature, can lead to wet quenching.
- The second zone, known as "operating zone", is characterized by intermediate values of τ_s (between 0.8 and 0.2) and an impregnation module greater than 10.
- The third zone, known as "fast drying zone", is characterized by high bed temperatures and low solvent saturation rates.

By fixing various values of IM and τ_s, and modifying the operating conditions, the deposit location can be chosen. For experiments A (IM = 400 $\tau_s = 0.78$) and B (IM = 80 and $\tau_s = 0.34$) noted in Fig. 1, realized at slow drying conditions, a uniform deposit is obtained. Scanning Electronic Microscopy micrograph presented in Fig. 2a illustrates this observation. Intermediate drying conditions, chosen for the

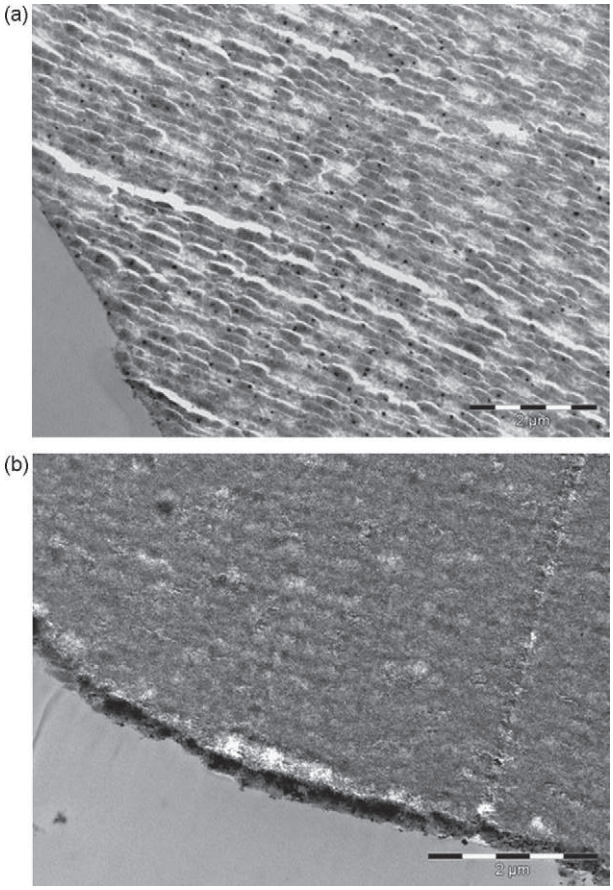

Fig. 2 – Deposit location according to the operating conditions ((a) experiment A and (b) experiment D).

experiment C (IM = 40, $\tau_s = 0.14$), permit to obtain a deposit concentrated at the particle periphery region. Experiment D (IM = 20, $\tau_s = 0.005$) corresponding to fast drying conditions leads to a deposit located only at the external particle surface (Fig. 2b).

In the study presented in this paper, another particulate support was tested in order to confirm and generalise the conclusions obtained concerning the effect of drying conditions on impregnation step of fine silica particle ($d_p < 150$–$200\,\mu m$). In this way, coarse porous alumina particles, $d_p \approx 2400\,\mu m$, were chosen.

2. Methods and materials

2.1. Experimental set-up

Depending on the metal source nature, the experiments can be carried out under air or controlled atmosphere (inert or reductive) in a batch fluidized bed. This reactor is a stainless steal cylindrical column with 0.1 m inner diameter and 0.5 m in height (Fig. 3).

The gas distributor is a stainless steel perforated plate with a porosity of 0.5%. The fluidizing gas flow rate is measured by a rotameter and preheated by an electrical heater before entering the bed. The elutriated particles and solvent vapours are collected at the column outlet, respectively by a cyclone and a condenser.

The metallic precursor solution is drawn up by a volumetric pump from a reservoir to an internal mixing two-fluid spray nozzle. The atomizing gas flow rate is controlled by a needle valve and measured by a rotameter. The bed temperature is controlled by means of a PID regulator. Monitoring of temperature and pressure drop takes place during operation.

Table 1 – Alumina characteristics

	Alumina
Mean diameter (mm)	2.4
Average pore diameter (Å)	45
Specific surface area, S_{BET} (m^2/g)	329
Pore volume (cm^3/g)	0.39
U_{mf} at 25 °C (minimal fluidization velocity) (m/s)	1.26

The solid sampling system is provided with a vacuum circuit and with a nitrogen circuit in order to sample under controlled atmosphere and to enable working with oxygen and water sensitive products.

The general experimental protocol is as follows:

- The column is initially charged with a fixed mass of porous particles (1 kg), which are then fluidized by a fixed gas flow rate.
- The spraying of pure solvent within the bed, at the same flow rate as for the metallic precursor solution, is carried out when the desired bed temperature is reached. As soon as thermal steady state regime is achieved the pure solvent is replaced by the solution containing the metallic precursor. Solid samples are removed from the bed at regular operation times.
- At the end of the impregnation process, the decomposition/activation of the precursors is carried out by stopping the spraying and by modifying both the fluidization gas composition (hydrogen/nitrogen mixture) and the bed temperature.

2.2. Supports and metal sources

The used porous support is γ alumina particles with a mean diameter about 2.4 mm. Its apparent density is about 2200 kg/m^3. Its other physical properties are presented in Table 1.

The impregnation solution is an aqueous solution of manganese tetrahydrate nitrate, $Mn(NO_3)_2{\cdot}4H_2O$ (20 wt.%).

2.3. Characterization methods

In order to determine the corresponding textural properties of the various samples, different characterization techniques were used such as

- Helium pycnometry (apparent and real bulk density).
- Mercury porosimetry (pore volume).
- N_2 adsorption–desorption (BET specific surface and pores size distribution).
- Scanning electron microscopy (SEM) (topology and morphology of the catalysts).
- Elemental analysis for metal content determination (metal loading).

From these analyses, three criteria were defined:

- Metal contents of the samples, resulting from elemental analysis. It allows determining real precursor contents using precursor chemical formula. The real impregnation rate, τ_{real}, is defined as the quantity of deposited precursor per unit mass of support.

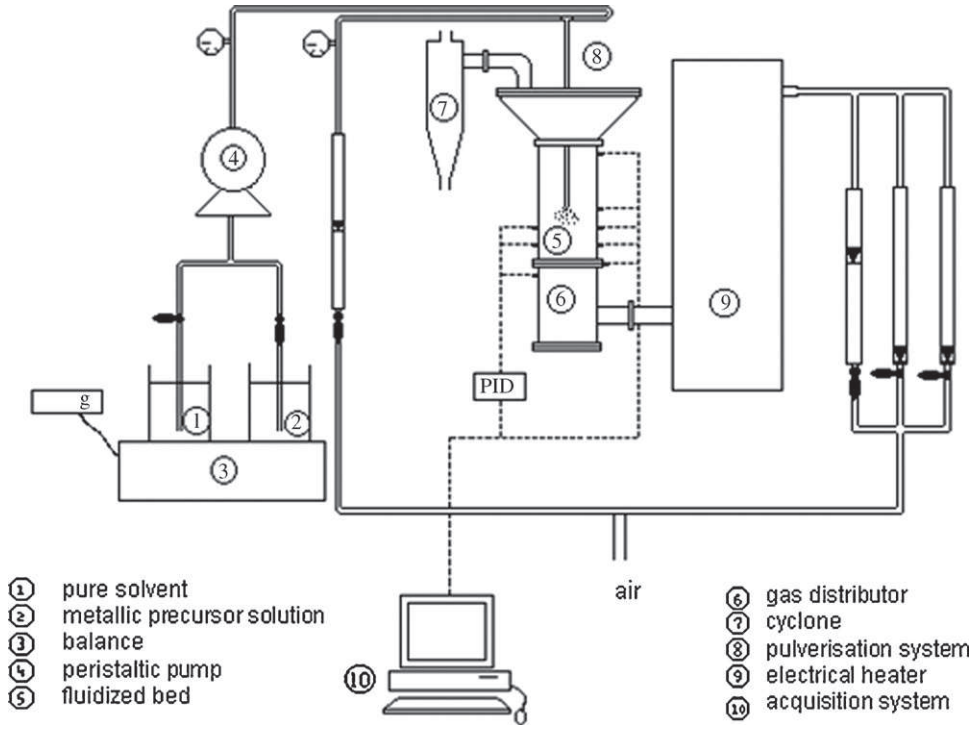

Fig. 3 – Experimental set-up.

- A theoretical impregnation rate, τ_{theo}. It corresponds to the ratio between the quantities of precursor sprayed during a time t and the mass of support present in the fluidized bed.

$$\tau_{theo} = 100\frac{\dot{m}_{so}C_l t}{m_s} \quad (5)$$

where $\dot{m}_{so}$ is the solution mass flow rate, C_l precursor concentration, t operation time, m_s initial weight of support in the bed.

- A porosity filling rate, τ_p, defined as

$$\tau_p = \frac{V_{pore}(t=0) - V_{pore}(t)}{V_{pore}(t=0)} \quad (6)$$

where $V_{pore}(t)$ and $V_{pore}(t=0)$ represent, respectively the particle pore volume determined at time t and at the initial time. These volumes were deduced from the cumulative pore size distribution, obtained by N_2 adsorption–desorption.

3. Operating conditions

To determine the effect of drying conditions two sets of experiments were carried out. Experimental conditions retained for these experiments are given in Table 2.

For experiment F, the impregnation was operated at 45 °C corresponding to fast drying (low liquid flow rate, low gas relative humidity in the reactor corresponding to $\tau_s = 0.08$, IM = 4). Experiment S, was carried out with a bed temperature about 27 °C, in "operating zone", corresponding to slow drying (high liquid flow rate and high gas relative humidity in the reactor equivalent to $\tau_s = 0.70$, IM = 11 > 10).

4. Results and discussion

For each experiment, theoretical and real impregnation rate evolutions were determined according to the impregnation time (Fig. 4).

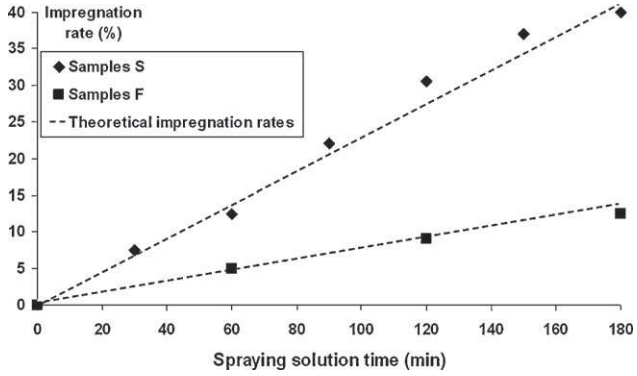

Fig. 4 – Theoretical and real impregnation rates versus pulverization time.

Whatever the operating conditions, the real impregnation rates evolve in a quasi linear way and are very close to the theoretical values. These results indicate that the whole sprayed nitrate is deposited on the porous solid particles. The deposit efficiency is nearly perfect. So, for a fixed solution flow rate, the operation time controls the metal content.

Samples removed from the bed at different operation times were analysed, permitting to characterize the evolution of the

Table 2 – Operating conditions of the two experiments

	Experiments	
	F	S
Fluidization gas flow rate (m^3/h)	28	31
Temperature gas entrance (°C)	60	78
Bed temperature (°C)	45	27
Solution pulverized flow rate (g/h)	187	740
Impregnation rate at the end of impregnation step (%)	12	40
IM	4	11
Saturation rate (τ_s)	0.08	0.70

Table 3 – Samples characteristics

	Samples				
	F1	S1	S2	S3	S4
Solvent evaporation type	Fast	Soft	Soft	Soft	Soft
Spraying solution time (h)	3	0.5	1	1.5	3
τ_{real} (%)	12.4	7.5	12.6	22	40
S_{BET} (m^2/g)	312	276	–	241	232
Pore volume (cm^3/g)	0.37	0.29	–	0.25	0.23
τ_p	0.05	0.25	–	0.36	0.41
IM	4	11	11	11	11
Solvent saturation rate (τ_s)	0.08	0.70	0.70	0.70	0.70

deposit repartition and the textural properties during operation (Table 3).

4.1. *Slow drying*

4.1.1. *Localisation and dispersion of manganese nitrate in the support*

After 3 h of calcination at 300 °C, the particles are cut, and the metallic oxide distribution on the external surface and on the cross-section of the samples is visualised using an optical microscope. Calcination permits to transform manganese nitrate in manganese oxide, which improves the contrast. The micrographs thus obtained are presented in Fig. 5.

These photographs show that the aqueous solution penetrates in the particles. Moreover, the precursor deposit inside the solid is similar to the displacement of a front from the periphery towards the particle centre (samples S1 to S3). This internal position of the impregnation front is a function of the impregnation rate. For samples S1 and S2, the precursor is rather on the particle borders (egg shell catalysts). For sample S3, the precursor reached the particle centre. The deposit is then uniform in the whole particle volume.

This phenomenon is comparable to that already observed during a heterogeneous reaction between a gas and a porous solid when the diffusion penetration time of the reactive gas is very high compared to the chemical reaction time (shrinking core model). In this case, the time evolution of the conversion rate, τ_{conv}, can be deduced from (Yagi and Kunii, 1955; Levenspiel, 1999):

$$\frac{t}{t_{dif}} = 1 - (1 - \tau_{conv})^{1/3} \quad (7)$$

where t_{dif} is the time for complete conversion.

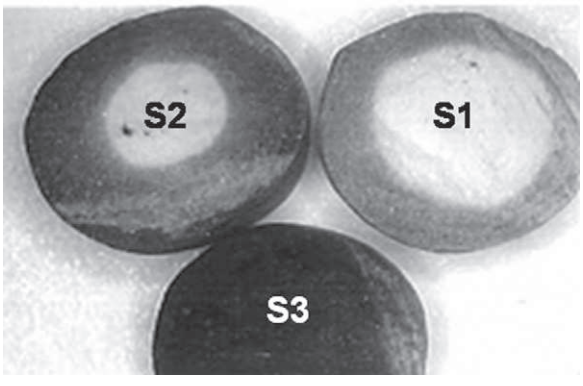

Fig. 5 – Microscope micrographs of samples S1, S2 and S3 (enlargement 50).

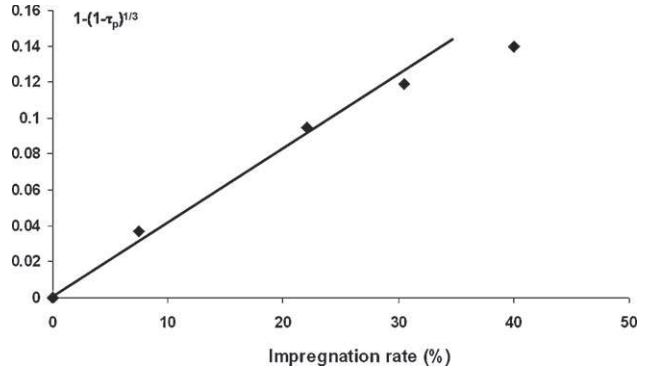

Fig. 6 – Evolution of $1 - (1 - \tau_p)^{1/3}$ versus time, shrinking core model (experiment S).

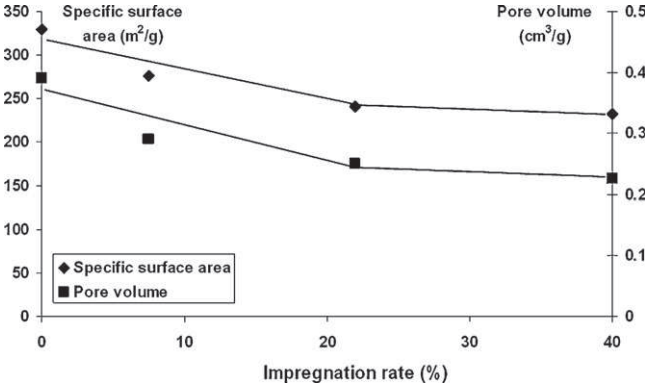

Fig. 7 – Pore volume and specific surface area versus impregnation rate.

This model is verified when the evolution of the term $1 - (1 - \tau_{conv})^{1/3}$, obtained from the experimental results, is a linear function of time. As the impregnation rate evolves linearly according to time, we have reported the evolution of $1 - (1 - \tau_p)^{1/3}$ versus to the impregnation rate (Fig. 6).

It is shown that evolution of the porosity filling rate, τ_p, versus time can be represented by a shrinking core model for impregnation rates lower than 30%. It is noticed that this value corresponds to 70–80% of the impregnation limit rate (found hereafter).

4.1.2. *Pore volume and specific surface evolution*

For slow drying conditions, the results presented in Table 3 and reproduced in Fig. 7 permit to conclude that the pore volume and specific surface area decrease when the impregnation rate increases.

It is noted that these two properties evolve in a linear way when the impregnation rate is les than 30% and stagnate for greater values. These results can be explained by the alumina structure, which can be represented by a pellet–grains model (Barby, 1976) having two porosity types (Fig. 8):

- Microporosity and mesoporosity on the level of the elementary grain.
- Mesoporosity and macroporosity in the intergranular space.

The deposit initially takes place in the elementary grain microporosity and mesoporosity. When this space is saturated with precursor, the deposit is then realized in the intergranular space. To estimate the elementary grains saturation limit, we considered two cases:

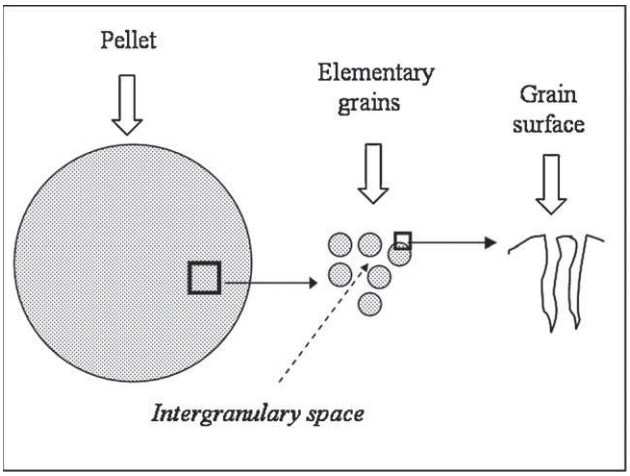

Fig. 8 – Schematic representation of a alumina particle according to the pellet–grains model.

- The elementary grain filled by a saturated precursor solution.
- The pore volume totally filled by tetrahydrate manganese nitrate crystals.

The estimation of the impregnation rates corresponding to these two borderline cases is based on the determination of alumina initial pore volume and density, the density of a saturated solution of manganese nitrate and the density of tetrahedral manganese nitrate in a solid form. The values of the filling rate thus obtained for these two limit cases are, respectively 29% and 44%. Experimental results show that for sample S4, containing 40 wt.% of manganese nitrate, the filling rate corresponds to 41% and the residual pore volume is equal to 0.23 cm^3/g.

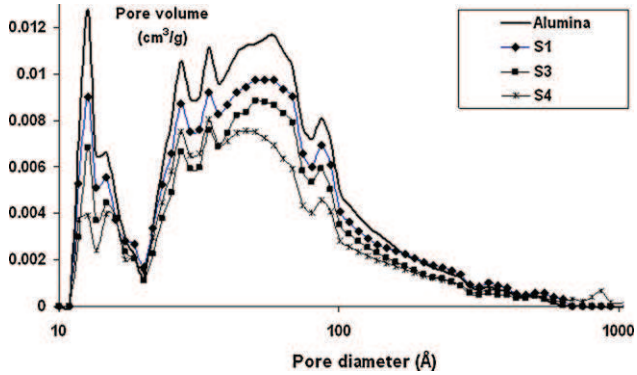

Fig. 9 – Pore size distribution (experiment S).

These results show that even at the end of the impregnation operation, all mesopore and micropore volumes available in the elementary grains of alumina particle are not filled by the crystallized solid. This finding leads to suppose that the limit of the dry impregnation process is fixed by the competition between dissolution and recrystallization of the precursor in the pores.

4.1.3. *Pore size distribution evolution*

In addition, the pore size distribution of the samples S1, S3 and S4 was presented (Fig. 9).

The pore size distribution pattern is conserved during the impregnation, but a pore volume regular reduction is

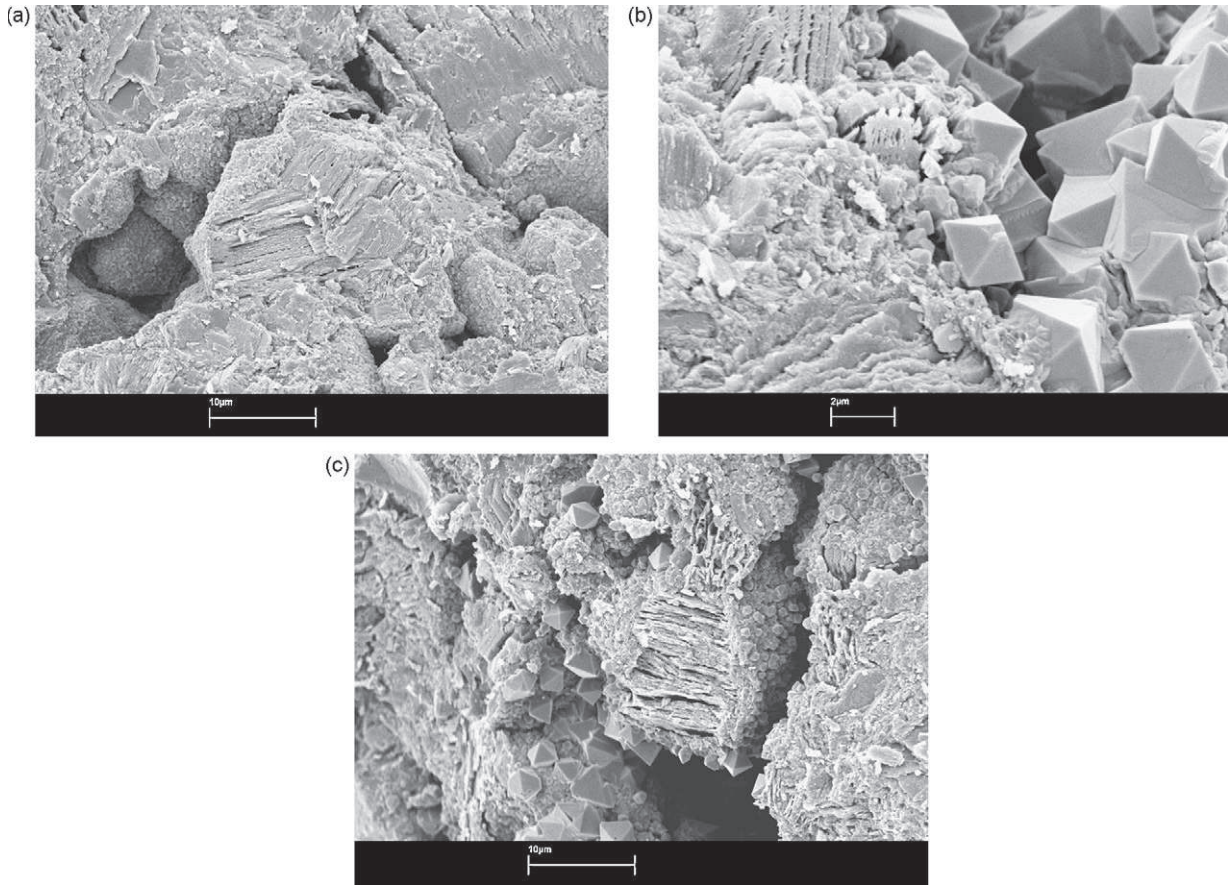

Fig. 10 – SEM micrographs of an impregnated alumina particle cross-section, sample S4 ((a) peripheral, (b) intermediate and (c) centre).

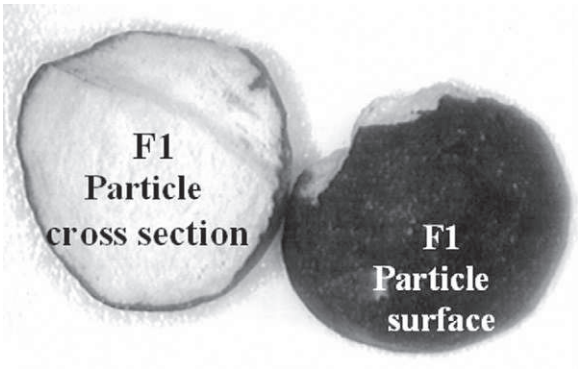

Fig. 11 – Microscope micrograph of sample F1 (enlargement 50).

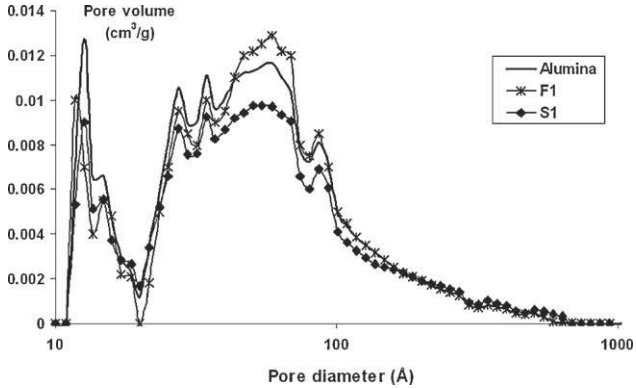

Fig. 12 – Pore size distribution of alumina, samples F1 and S1.

observed. These observations, coupled with the existence of an impregnation front characterized by a "shrinking core" model and the alumina structure (pellet–grains), permit to suppose that this phenomenon is directly related to the reduction of the virgin elementary grains number in the alumina particle during the operation (virgin means that the elementary grain does not contain precursor). So, the elementary grain impregnation mechanism at local scale, due to capillary suction, is independent of its position in the particle.

4.1.4. *Scanning electron microscopy (SEM) observation*

After a calcination step, the particle cross-section was observed by SEM. Two cases can be distinguished:

- When the impregnation rate is lower than 20–25%, the size of the metallic oxide nanoparticles is less than 5 nm and is not detected by SEM analysis. In this case, we can suppose that the deposit takes place essentially in the micropores and mesopores of the alumina particles (inside the elementary grains).
- When the impregnation rate is higher than 35% (experiments S4), the SEM observations realized in different regions of the particles (peripheral, intermediate and central), indicate a significant morphology modification (Fig. 10).

In the intermediate and central region, octahedral form crystalline structures, corresponding to pyrolusite manganese oxide, are detected. The presence of these large crystalline structures (0.5–2 μm) indicates that in this case, $\tau_{real} > 35\%$, the deposit takes place partly in the interstitial spaces. So the crystallite size is controlled by the macropore steric effect ($d_{pore} > 300$ nm).

This morphology is not observed in particle peripheral zone. This indicates the significant effect of the precursor local concentration and the drying rate on the size and morphology of the crystals. Indeed, on the particle surface, the weak precursor concentration and high drying rate can produce crystals with a smaller size, which cannot be detected by SEM.

4.2. *Fast drying*

For fast drying conditions, microscopy micrographs of the external surface and cross-section of the solid samples, obtained at the end of experiment F, are presented in Fig. 11.

The deposit, characterized by the most darkened zones, is located on the particle surface, but the intermediate and central zones remain virgin. The results presented in Tables 1 and 3, concerning pore volume sand specific surface area indicate that these properties are fairly affected by the manganese nitrate deposit (comparison between sample F1 and initial alumina). The pore volume decreases from 0.39 to 0.37 cm^3/g and the specific surface area from 329 to 312 m^2/g.

The comparison between samples F1 and S1, having an almost same impregnation rate, indicates that in case of slow drying (sample S1), the pore filling rate is 5 times higher than that of sample F1. This phenomenon is confirmed by the observation of Fig. 12 representing the pore size distribution of alumina particles, samples F1 and S1.

5. Conclusion

The experiments realized with coarse alumina particles enabled to better characterize and understand the impregnation processes.

When impregnation is carried out under slow drying conditions (IM = 11 and $\tau_s = 0.70$), the solid precursor deposit takes place inside the particles. In this situation, two deposit morphologies are distinguished:

- For impregnation rates lower than 20%, the deposit takes place in the elementary grain. The size of the metallic oxide nanoparticles is less than the average pore size value < 5 nm). The impregnation kinetics can be represented by a "shrinking core" model.
- For impregnation rates higher than 35%, the elementary grains contains the metallic oxide nanoparticles and the interstitial grain spaces contains micronic particles. Large crystals are observed in the macroporosity existing in the central areas of the particles where the drying rate is low.

When impregnation is realized under fast drying conditions (IM = 4 and $\tau_s = 0.08$), the deposit is then located on the particle external surface (egg shell catalysts). Moreover the deposit does not have a notable effect on the solid porosity.

These findings enable to generalise the conclusions concerning the dry impregnation of fine porous particles by metallic salts to the coarse porous particles. It indicates that dry impregnation in fluidized beds is very flexible and, by a simple modification of the operating conditions, one can fix the deposit location.

References

Barby, D., 1976, in Parfitt, G.D. and Sing, K.S.W., Sing, K.S.W. (eds) (p. 353).

Barthe, L., 2007, Synthèse et dépôt de nanoparticules métalliques dans un support poreux par imprégnation en voies sèche dans un lit fluidisé: élaboration de catalyseurs supportés, PhD thesis, INP Toulouse.

Barthe, L., Desportes, S., Hemati, M., Philippot, K. and Chaudret, B., 2007, Synthesis of supported catalysts by dry impregnation in fluidized bed. Chem Eng Res Des, 85(A6): 1–11.

Burdine, N.T., 1953, Relative permeability calculations from pore size distribution data. Pet. Trans. Am. Inst. Min. Eng., 198: 71–77.

Desportes, S., 2005, Imprégnation en voie sèche en lit fluidisé, application à la synthèse de catalyseurs supportés, PhD thesis, INP, Toulouse.

Desportes, S., Steinmetz, D., Hemati, M., Philippot, K. and Chaudret, B., 2005, Production of supported asymmetric catalysis in a fluidized bed. Powder Technol., 157: 12–19.

Fulton, J.W., 1986, Selecting the catalyst configuration. Chem. Eng., 93: 97–101.

Lekhal, A., Glasser, B. and Khinast, J.G., 2001, Impact of drying on catalyst profile of supported impregnation catalysts. Chem. Eng. Sci., 56(15): 4473–4487.

Levenspiel, O., (1999). *Chemical Reaction Engineering* (3rd ed.). (Wiley, New York).

Yagi, S. and Kunii, D., 1955, Studies on combustion of carbon particles in flames and fluidized beds, In *Fifth Symposium (International) on Combustion* , pp. 231–244.